







Gallium phosphide-on-insulator integrated photonic structures fabricated using micro-transfer printing

MAXIMILIEN BILLET,^{1,2,3,*} LUIS REIS,^{1,2,3} YOAN LÉGER,⁴ 
CHARLES CORNET,⁴  FABRICE RAINERI,⁵ ISABELLE SAGNES,⁵ 
KONSTANTINOS PANTZAS,⁵  GRÉGOIRE BEAUDOIN,⁵ GUNTHER
ROELKENS,^{1,2} FRANCOIS LEO,³ AND BART KUYKEN^{1,2}

¹Photonics Research Group, Department of Information Technology, Ghent University IMEC, Ghent B-9000, Belgium Photonics Research Group, Ghent University-IMEC, Ghent, Belgium

²Center for Nano- and Biophotonics (NB-Photonics), Ghent University, Ghent, Belgium

³OPERA-Photonique, Université libre de Bruxelles, Brussels, Belgium

⁴Université Rennes, INSA Rennes, CNRS, Institut FOTON – UMR 6082, F-35000 Rennes, France

⁵Centre de Nanosciences et de Nanotechnologies (C2N), CNRS, Université Paris Saclay, F-91120 Palaiseau, France

*maximilien.billet@ugent.be

Abstract: Gallium phosphide-on-insulator emerged recently as a promising platform for integrated nonlinear photonics due to its intrinsic material properties. However, current integration solutions, using direct die-to-wafer bonding, do not support spatially localized integration with CMOS circuits which induce a large and expensive footprint material need. Here we demonstrate the transfer of gallium phosphide layers to an oxidized silicon wafer using micro-transfer printing as a new approach for versatile future (hybrid) integration. Using this novel approach, we demonstrate as a proof of concept the fabrication of gallium phosphide-on-insulator ring resonators with Q-factors as high as 35,000.

© 2022 Optica Publishing Group under the terms of the [Optica Open Access Publishing Agreement](#)

1. Introduction

The integration of nonlinear photonic functionalities has recently drawn increasing interest as it provides scalable, compact, and low-cost solutions based on the Kerr effect such as supercontinuum [1,2] and frequency comb [3–6], or based on the second order nonlinearity such as frequency conversion [7,8]. Silicon-on-insulator (SOI) has proven an efficient platform for its high material quality and its compatibility with the CMOS industry [9]. The enhanced device nonlinearity induced by the strong optical field confinement and the low linear loss coming from the mature silicon fabrication technology enable various nonlinear applications [4,10–12]. However, silicon suffers from the lack of second order nonlinearity and from nonlinear loss (two-photon absorption) at telecom wavelengths, which strongly limits the range of applications. In this context, wide-bandgap III-V semiconductors such as aluminum nitride (AlN), gallium nitride (GaN) or gallium phosphide (GaP), which lack two-photon absorption at telecom wavelengths, constitute alternatives for implementing nonlinear functions [7,13,14]. On top of a strong Kerr response, these materials also possess a strong $\chi^{(2)}$ nonlinearity. Gallium phosphide, in particular, is a promising material owing to its high refractive index of 3.05, very large $\chi^{(2)}$ and $\chi^{(3)}$ coefficients and a transparency window which ranges from the visible to the long-infrared wavelengths (0.55 μm to 11 μm) [15–18].

In the case of GaP, the strong confinement of the light can be realized in several ways. The GaP layer can be suspended [19,20], but this technique is difficult to scale. Alternatively, it can be achieved by exploiting the strong refractive index contrast between the III-V material

and an insulator layer, as was recently demonstrated using a die-to-wafer bonding approach [15]. Although the technique allows for wafer scale integration it demands a large III-V material footprint and is less compatible with hybrid integration. Table 1 summarizes the current approaches in literature related to high confinement GaP photonic structures.

Table 1. Overview of the existing solutions for GaP integrated photonics

Reference	GaP material	GaP integration	Losses (dB/mm)	Q-factor	Nonlinear effect
[15]	GaP/AlGaP/GaP MOCVD	Direct die-to-wafer bonding	0.1	>100.000	Kerr-frequency comb and frequency doubling in microrings
[16]	GaP/GaAs MOCVD	Direct die-to-wafer bonding	2.6	No data	Second harmonic generation in nanowaveguides
[17]	GaP/AlGaP/GaP	Membrane releasing in solution and direct bonding	1.5	40.000 (fundamental) 16.000 (SH)	Second harmonic generation in ring resonators
[18]	No data	Releasing of GaP microdisks	No data	110.000 (fundamental) 10.000 (SH)	Second harmonic generation in suspended microdisks
[19]	GaP/AlGaP/GaP MOCVD	Releasing of suspended membranes	4.0	No data	Cascaded four wave mixing in suspended photonic crystals
[20,21]	GaP/Si MBE	Microdisk undercutting on silicon pedestal	No data	10.000	Second harmonic generation with random quasi-phase matching

In this work we propose micro-transfer printing (μ TP) of GaP coupons as a novel approach for GaP hybrid integration. This method has already proven its versatility in different electronic, optoelectronic and photonic micro-systems [22–24]. Recently, it has been used for the fabrication of heterogeneous III-V/Si lasers by transfer printing III-V semiconductor optical amplifiers on silicon [25] and silicon nitride (SiN) passive waveguide circuits [26].

Micro-transfer printing can be done on any kind of substrate (oxidized wafers, electronic and photonic integrated circuits). Furthermore, the required material quantity is small as the size of the coupon required for transfer is similar to that of the device. This method also allows for a high level of heterogeneous integration, as different materials (active or passive) can be printed on the same target. Finally, it is also possible to print identical coupons from the same wafer source on different targets. For example, [26,27] show same optical amplifier devices coming from the same source printed on different platforms, once on SiN and once on lithium niobate.

Here we demonstrate the fabrication of a GaP-on-insulator (GaP-OI) integrated photonic platform using the printing of GaP layers on an oxidized silicon substrate. These layers are patterned into GaP-OI microring resonators, the quality of which is characterized and compared against the state of the art.

2. Micro-transfer printing technology

Micro-transfer printing is a technology that allows for heterogeneous integration with a high flexibility in term of material choice. The method consists in the fabrication of a source wafer, presenting coupons that can be picked and printed on a target substrate. The principle of μ TP is schematically illustrated in Fig. 1(a). The process starts with the fabrication of the coupons on a source material wafer, a III-V stack in our case, which includes the material to transfer, grown on top of a sacrificial release layer. The coupons are patterned using optical lithography, and wet/dry etching. Then, the release layer is etched in a chemical solution which is highly selective towards

the material and the substrate. The structure remains suspended by very thin mechanical tethers. Then, the coupons are picked using a polydimethylsiloxane (PDMS) stamp. The stamp adhesion to the coupon depends on the velocity by which the stamp is retracted [28]. The coupons are picked-up with sufficient velocity to break the tethers.

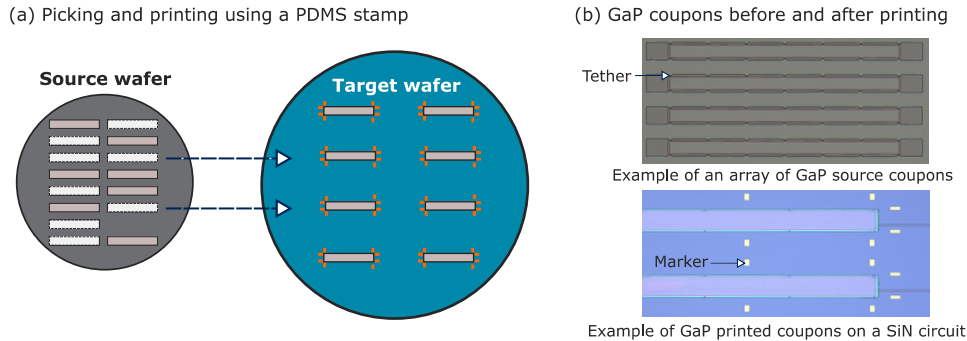


Fig. 1. (a) Overview of the micro-transfer printing concept showing a source wafer with suspended coupons and a host target. (b) GaP coupons when released on the source wafer and after picking and printing on a SiN target circuit.

A microscope with a mechanical motorized moving stage allows to drive the stamp onto the target wafer. The coupons are printed by laminating the stamp to the target, shifting the stamp by a few micrometers to break adhesion, and, finally, slowly removing the stamp. Several hybrid integrated photonic devices have been demonstrated using μ TP technology, including semiconductor optical amplifiers, photodiodes, or nonlinear devices [29–32]. An example of GaP coupons before and after printing on a SiN circuit can be seen in Fig. 1(b). In the following section, the complete process flow for GaP μ TP hybrid integration is given in greater detail.

3. Process flow for GaP transfer printing

The first step is the fabrication of suspended rectangular GaP coupons ($1 \text{ mm} \times 60 \mu\text{m}$), anchored by mechanical tethers. The material stack is grown on top of a GaP substrate by metal organic vapor phase epitaxy (MOVPE) and consists of a 300 nm GaP layer on top of a $1 \mu\text{m}$ aluminum gallium phosphide (AlGaP) release layer (Fig. 2(a)). A first layer of 500 nm of amorphous silicon (a-Si) is deposited using plasma-enhanced chemical vapor deposition (Fig. 2(b)). This layer serves as a hard mask for the following step. The rectangles are patterned with UV-lithography. To access the GaP substrate, the pattern is transferred in the a-Si and III-V stacks with reactive ion etching (RIE) and inductively coupled plasma - reactive ion etching (ICP-RIE). A HCl dip is used to clean remaining residues of AlGaP (Fig. 2(c)). The coupons are then encapsulated in a second a-Si layer of 500 nm (Fig. 2(d)). The mechanical tethers are patterned in the a-Si using UV lithography and RIE etching. The tethers have a $2 \mu\text{m}$ wide breakable part and need to be positioned every $100 \mu\text{m}$. The coupons are released by placing them for 3 hours in a 3%-hydrofluoric (HF) solution selectively etching the AlGaP release layer (Fig. 2(e)). At this point the coupons are suspended and can be picked up using the PDMS stamp (Fig. 2(f)). In our experiment, a yield of 90% of picking is achieved, and could be increased by using more advanced design of coupons. Simultaneously, a target wafer is prepared. The target is a 300 nm oxide layer on top of a silicon substrate. Metallic markers are placed on the target using UV-lithography and lift-off. These markers serve as a reference system to pattern the printed coupons. An adhesive DVS-BCB layer of 500 nm is spin coated on the target and is baked at 150°C for 10 min. The coupons are then printed using an X-Celeprint micro-transfer printing tool (Fig. 2(g)). Every successfully picked coupons can be print in that case. To enhance the adhesion

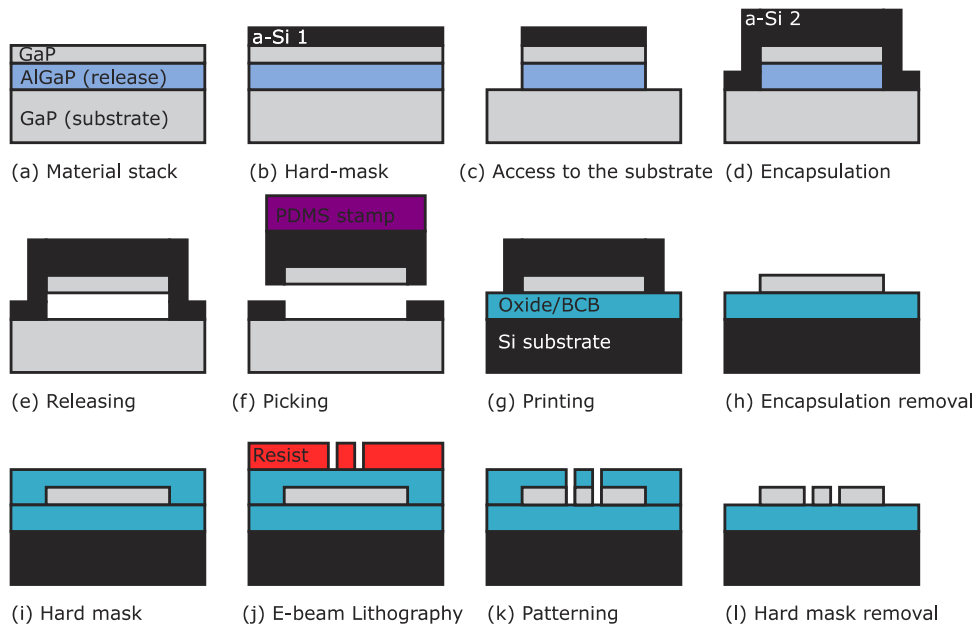


Fig. 2. Complete process flow for GaP-OI integrated waveguide fabrication using micro-transfer printed GaP layers. Details in the text.

between the coupons and the target, the target substrate is heated at 70 °C during the printing. After printing, the BCB is baked again at a temperature of 280 °C for 1 hour and under vacuum. The hard cure is typically carried out as final cure after all polymer layers of the device structure have been completed. Finally, the a-Si encapsulation is removed (Fig. 2(h)). Around 80% of

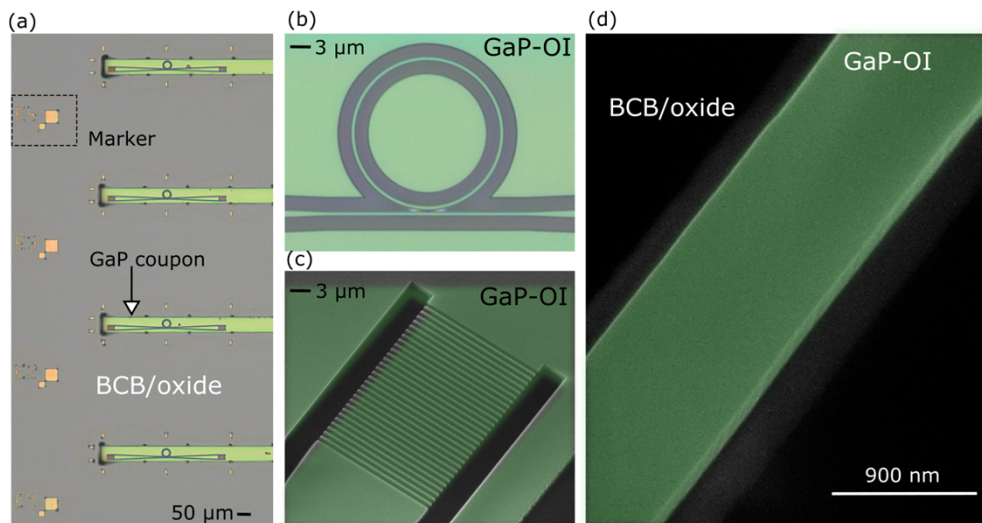


Fig. 3. (a) Optical-microscopy micrographs of GaP-OI optical waveguides and ring resonators fabricated using transfer-printed GaP layers. (b-d) colorized SEM micrographs showing details of the ring and waveguides (see text for details).

the a-Si is etched with RIE and the remaining thin a-Si film is selectively etched in a 30% KOH solution heated at 85 °C.

The second part of the process consists in the patterning of the waveguides. An oxide hard mask of 300 nm is deposited by plasma-enhanced chemical vapor deposition on the GaP layer (Fig. 2(i)). The waveguide patterns are defined through electron-beam lithography using an ARP 6200 series positive resist and a conductive protective coating of PMMA Electra 92 (Fig. 2(j)). The patterns are then transferred into the oxide hard mask using RIE (Fig. 2(k)). The resist is removed with acetone and oxygen plasma. The patterns of the oxide hard-mask are then transferred into the GaP layer using RIE-ICP dry etching (Fig. 2(k)). The last step of the process flow consists in stripping the oxide mask away in a buffered HF solution for 5 min (Fig. 2(l)). Figure 3(a) shows GaP ring resonators fabricated following the above process flow. The different parts of the devices, i.e., the ring (Fig. 3(b)), the grating coupler (Fig. 3(c)) and the waveguide (Fig. 3(d)) are shown with a higher degree of magnification.

4. Characterization of GaP-OI microrings

To test the platform, we fabricated a GaP-OI microring resonator. The dimensions of the bus waveguide and the ring waveguide are 300 nm thick and 800 nm wide. The coupling gap is designed to target critical coupling and is 250 nm. The optical response of the ring is measured at telecom wavelengths using a continuous wave tunable laser. Light is coupled into the waveguide through grating couplers (period of 900 nm and fill factor of 0.4). A polarization controller is inserted between the laser and the grating coupler to excite the TE mode of the waveguide. The transmitted power is then collected by a power-meter. Typical values of insertion losses for the gratings are measured to be 15 dB/coupler. Our results are shown in Fig. 4(a). Several resonances are recorded, with a free spectral range of 922.64 GHz, in accordance with the theoretical group index of 3.45. The extinction ratio is more than 8.5 dB showing that we are near the critical coupling condition. The quality-factor (Q-factor) of each resonance was extracted following the method described in Ref. [33]. The resonance line with the highest Q-factor of 40 100 is shown in Fig. 4(b). The average value of the Q-factor is 35 000 with a standard deviation of 5000. The propagation loss in our platform is higher than the state of the art but could be improve by using higher quality lithography and etching recipes [15]. Furthermore the roughness at the bottom surface of the GaP material induced by the long releasing time (3 hours) is limiting the quality of our platform, but could be drastically reduced by using advanced design of coupons including an etching hole array making the releasing time much more shorter (few minutes). Nevertheless, GaP ring resonators with Q-factor around 40 000 can be harnessed for nonlinear functionalities

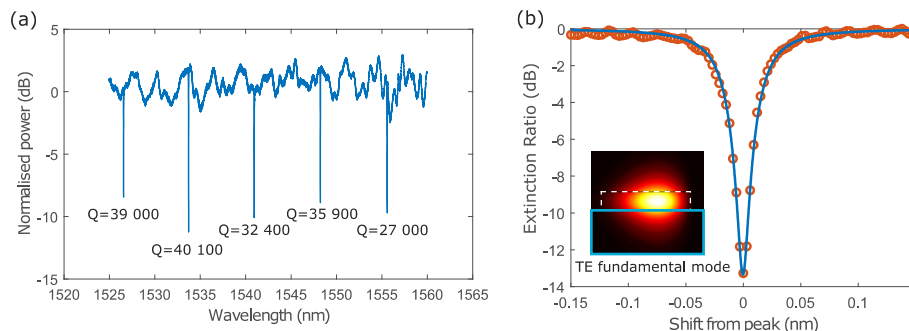


Fig. 4. (a) Measurements of microring resonance lines. (b) Focus on the finest resonance line for a wavelength of 1534 nm. The red dots show the measurement data and the blue curve is a fit using the model from Ref. [33]. The inset is a simulation of the field distribution for the fundamental TE mode in this ring resonator.

[17]. Combined with the versatility of the printing approach, our platform has a strong potential for applications that require dense integration of complex photonic structures.

5. Discussion and conclusion

In the past, III-V materials have been used for many nonlinear photonic applications such as second harmonic generation (SHG) [34–36], Kerr frequency comb [6] or supercontinuum generation [37]. In order to use high confinement GaP platform in the future for similar applications, we demonstrate in this work the micro-transfer printing of GaP coupons on an insulator layer. Using this novel integration approach, we fabricated GaP-on-insulator ring resonators with an average Q-factor of 35 000. Nonlinear experiments could potentially now be carried out in this platform and the versatility of the micro-transfer printing approach can bring these functionalities to more complex structures, paving the way for the next generation of integrated photonic circuits.

Funding. Agence Nationale de la Recherche (17-CE24-0019, ORPHEUS, RENATECH network); Fonds De La Recherche Scientifique - FNRS; European Research Council (No. 726420, No. 757800, No. 759483).

Acknowledgments. We would like to thank Muhammad Muneeb for helping with e-beam processing.

Disclosures. The authors declare no conflicts of interest.

Data availability. Data underlying the results presented in this paper are not publicly available at this time but may be obtained from the authors upon reasonable request.

References

1. H. Guo, C. Herkommer, A. Billat, D. Grassani, C. Zhang, M. H. P. Pfeiffer, W. Weng, C.-S. Brès, and T. J. Kippenberg, “Mid-infrared frequency comb via coherent dispersive wave generation in silicon nitride nanophotonic waveguides,” *Nat. Photonics* **12**(6), 330–335 (2018).
2. R. Halir, Y. Okawachi, J. S. Levy, M. A. Foster, M. Lipson, and A. L. Gaeta, “Ultrabroadband supercontinuum generation in a CMOS-compatible platform,” *Opt. Lett.* **37**(10), 1685–1687 (2012).
3. T. J. Kippenberg, R. Holzwarth, and S. A. Diddams, “Microresonator-based optical frequency combs,” *Science* **332**(6029), 555–559 (2011).
4. A. G. Griffith, R. K. W. Lau, J. Cardenas, Y. Okawachi, A. Mohanty, R. Fain, Y. H. D. Lee, M. Yu, C. T. Phare, C. B. Poitras, A. L. Gaeta, and M. Lipson, “Silicon-chip mid-infrared frequency comb generation,” *Nat. Commun.* **6**(1), 6299 (2015).
5. L. Chang, W. Xie, H. Shu, Q.-F. Yang, B. Shen, A. Boes, J. D. Peters, W. Jin, C. Xiang, S. Liu, G. Moille, S.-P. Yu, X. Wang, K. Srinivasan, S. B. Papp, K. Vahala, and J. E. Bowers, “Ultra-efficient frequency comb generation in AlGaAs-on-insulator microresonators,” *Nat. Commun.* **11**(1), 1331 (2020).
6. M. Pu, L. Ottaviano, E. Semenova, and K. Yvind, “Efficient frequency comb generation in AlGaAs-on-insulator,” *Optica* **3**(8), 823–826 (2016).
7. A. W. Bruch, X. Liu, X. Guo, J. B. Surya, Z. Gong, L. Zhang, J. Wang, J. Yan, and H. X. Tang, “17 000%/W second-harmonic conversion efficiency in single-crystalline aluminum nitride microresonators,” *Appl. Phys. Lett.* **113**(13), 131102 (2018).
8. J. Lu, J. B. Surya, X. Liu, A. W. Bruch, Z. Gong, Y. Xu, and H. X. Tang, “Periodically poled thin film lithium niobate microring resonators with a second-harmonic generation efficiency of 250,000%/W,” arXiv:1911.00083 [physics, physics:quant-ph] (2019).
9. A. Rahim, J. Goyvaerts, and B. Szlag, *et al.*, “Open-access silicon photonics platforms in Europe,” *IEEE J. Sel. Top. Quantum Electron.* **25**(5), 1–18 (2019).
10. B. Kuyken, T. Ideguchi, S. Holzner, M. Yan, T. W. Hänsch, J. Van Campenhout, P. Verheyen, S. Coen, F. Leo, R. Baets, G. Roelkens, and N. Picqué, “An octave-spanning mid-infrared frequency comb generated in a silicon nanophotonic wire waveguide,” *Nat. Commun.* **6**(1), 6310 (2015).
11. M. Yu, Y. Okawachi, A. G. Griffith, M. Lipson, and A. L. Gaeta, “Mode-locked mid-infrared frequency combs in a silicon microresonator,” *Optica*, *Optica* **3**(8), 854–860 (2016).
12. J. Wei, C. Cret, M. Billet, F. Leo, B. Kuyken, and S.-P. Gorza, “Supercontinuum generation assisted by wave trapping in dispersion-managed integrated silicon waveguides,” *Phys. Rev. Appl.* **14**(5), 054045 (2020).
13. E. Stassen, M. Pu, E. Semenova, E. Zavarin, W. Lundin, and K. Yvind, “High-confinement gallium nitride-on-sapphire waveguides for integrated nonlinear photonics,” *Opt. Lett.* **44**(5), 1064–1067 (2019).
14. C. Xiong, W. Pernice, K. K. Ryu, C. Schuck, K. Y. Fong, T. Palacios, and H. X. Tang, “Integrated GaN photonic circuits on silicon (100) for second harmonic generation,” *Opt. Express* **19**(11), 10462–10470 (2011).
15. D. J. Wilson, K. Schneider, S. Hönl, M. Anderson, Y. Baumgartner, L. Czornomaz, T. J. Kippenberg, and P. Seidler, “Integrated gallium phosphide nonlinear photonics,” *Nat. Photonics* **14**(1), 57–62 (2020).

16. A. P. Anthur, H. Zhang, Y. Akimov, J. R. Ong, D. Kalashnikov, A. I. Kuznetsov, and L. Krivitsky, "Second harmonic generation in gallium phosphide nano-waveguides," *Opt. Express* **29**(7), 10307–10320 (2021).
17. A. D. Logan, M. Gould, E. R. Schmidgall, K. Hestroffer, Z. Lin, W. Jin, A. Majumdar, F. Hatami, A. W. Rodriguez, and K.-M. C. Fu, "400%/W second harmonic conversion efficiency in 14 μm -diameter gallium phosphide-on-oxide resonators," *Opt. Express* **26**(26), 33687–33699 (2018).
18. D. P. Lake, M. Mitchell, H. Jayakumar, L. F. dos Santos, D. Curic, and P. E. Barclay, "Efficient telecom to visible wavelength conversion in doubly resonant gallium phosphide microdisks," *Appl. Phys. Lett.* **108**(3), 031109 (2016).
19. A. Martin, S. Combri , A. de Rossi, G. Beaudoin, I. Sagnes, and F. Raineri, "Nonlinear gallium phosphide nanoscale photonics [Invited]," *Photonics Res.* **6**(5), B43–B49 (2018).
20. P. Guillem , Y. Dumeige, J. Stodolna, M. Vallet, T. Rohel, A. L toublon, C. Cornet, A. Ponchet, O. Durand, and Y. L ger, "Second harmonic generation in gallium phosphide microdisks on silicon: from strict 4 to random quasi-phase matching," *Semicond. Sci. Technol.* **32**(6), 065004 (2017).
21. R. Saleem-Urothodi, J. L. Pouliquen, T. Rohel, R. Bernard, C. Pareige, A. Lorenzo-Ruiz, A. Beck, A. L toublon, O. D. Sagazan, C. Cornet, Y. Dumeige, and Y. L ger, "Loss assessment in random crystal polarity gallium phosphide microdisks grown on silicon," *Opt. Lett.* **45**(16), 4646–4649 (2020).
22. K. J. Lee, J. Lee, H. Hwang, Z. J. Reitmeier, R. F. Davis, J. A. Rogers, and R. G. Nuzzo, "A printable form of single-crystalline gallium nitride for flexible optoelectronic systems," *Small* **1**(12), 1164–1168 (2005).
23. L. Zhang, C. Zhang, Z. Tan, J. Tang, C. Yao, and B. Hao, "Research progress of microtransfer printing technology for flexible electronic integrated manufacturing," *Micromachines* **12**(11), 1358 (2021).
24. S. Lee, B. Kang, H. Keum, N. Ahmed, J. A. Rogers, P. M. Ferreira, S. Kim, and B. Min, "Heterogeneously Assembled Metamaterials and Metadevices via 3D Modular Transfer Printing," *Sci. Rep.* **6**(1), 27621 (2016).
25. B. Haq, J. R. Vaskasi, J. Zhang, A. Gocalinska, E. Pelucchi, B. Corbett, G. Roelkens, and G. Roelkens, "Micro-transfer-printed III-V-on-silicon C-band distributed feedback lasers," *Opt. Express* **28**(22), 32793–32801 (2020).
26. C. O. de Beeck, B. Haq, L. Elsinger, A. Gocalinska, E. Pelucchi, B. Corbett, G. Roelkens, and B. Kuyken, "Heterogeneous III-V on silicon nitride amplifiers and lasers via microtransfer printing," *Optica* **7**(5), 386–393 (2020).
27. C. O. de Beeck, F. M. Mayor, S. Cuyvers, S. Poelman, J. F. Herrmann, O. Atalar, T. P. McKenna, B. Haq, W. Jiang, J. D. Witmer, G. Roelkens, A. H. Safavi-Naeini, R. V. Laer, and B. Kuyken, "III/V-on-lithium niobate amplifiers and lasers," *Optica* **8**(10), 1288–1289 (2021).
28. H. Cheng, M. Li, J. Wu, A. Carlson, S. Kim, Y. Huang, Z. Kang, K.-C. Hwang, and J. A. Rogers, "A viscoelastic model for the rate effect in transfer printing," *J. Appl. Mechanics* **80**(4), 041019 (2013).
29. J. Zhang, G. Muliuk, and J. Juvert, *et al.*, "III-V-on-Si photonic integrated circuits realized using micro-transfer-printing," *APL Photonics* **4**(11), 110803 (2019).
30. J. Goyvaerts, S. Kumari, S. Uvin, J. Zhang, R. Baets, A. Gocalinska, E. Pelucchi, B. Corbett, and G. Roelkens, "Transfer-print integration of GaAs p-i-n photodiodes onto silicon nitride waveguides for near-infrared applications," *Opt. Express* **28**(14), 21275–21285 (2020).
31. M. Billet, Y. L ger, C. Cornet, F. Raineri, I. Sagnes, G. Roelkens, F. Leo, and B. Kuyken, "Gallium phosphide on insulator photonics enabled by micro-transfer printing," in *OSA Advanced Photonics Congress (AP) 2020 (IPR, NP, NOMA, Networks, PVLED, PSC, SPPCom, SOF) (2020), Paper ITu2A.6* (Optical Society of America, 2020), p. ITu2A.6.
32. T. Vanackere, M. Billet, C. O. de Beeck, S. Poelman, G. Roelkens, S. Clemmen, and B. Kuyken, "Micro-transfer printing of lithium niobate on silicon nitride," in *2020 European Conference on Optical Communications (ECOC) (2020)*, pp. 1–4.
33. W. Bogaerts, P. D. Heyn, T. V. Vaerenbergh, K. D. Vos, S. K. Selvaraja, T. Claes, P. Dumon, P. Bienstman, D. V. Thourhout, and R. Baets, "Silicon microring resonators," *Laser Photonics Rev.* **6**(1), 47–73 (2012).
34. N. Poulvellarie, U. Dave, K. Alexander, C. Ciret, M. Billet, C. Mas Arabi, F. Raineri, S. Combri , A. De Rossi, G. Roelkens, S.-P. Gorza, B. Kuyken, and F. Leo, "Second-harmonic generation enabled by longitudinal electric-field components in photonic wire waveguides," *Phys. Rev. A* **102**(2), 023521 (2020).
35. C. Ciret, K. Alexander, N. Poulvellarie, M. Billet, C. M. Arabi, B. Kuyken, S.-P. Gorza, and F. Leo, "Influence of longitudinal mode components on second harmonic generation in III-V-on-insulator nanowires," *Opt. Express* **28**(21), 31584–31593 (2020).
36. L. Chang, A. Boes, P. Pintus, J. D. Peters, M. Kennedy, X.-W. Guo, N. Volet, S.-P. Yu, S. B. Papp, and J. E. Bowers, "Strong frequency conversion in heterogeneously integrated GaAs resonators," *APL Photonics* **4**(3), 036103 (2019).
37. B. Kuyken, M. Billet, F. Leo, K. Yvind, and M. Pu, "Octave-spanning coherent supercontinuum generation in an AlGaAs-on-insulator waveguide," *Opt. Lett.* **45**(3), 603–606 (2020).